Molecular-dynamics simulation of a model with incommensurate phases

Krzysztof Parlinski*
Institut für Festkörperforschung, Kernforschungsanlage Jülich, D-5170 Jülich, Federal Republic of Germany
(Received 9 July 1986)

Two-dimensional models of displacive and order-disorder behavior, in the form of crystallites with free boundary conditions and with one-dimensional incommensurate and/or commensurate phases, have been studied using the molecular-dynamics method. The incommensurate phase can be characterized with any wave vector by the appropriate choice of potential-energy parameters. The ground-state devil's staircases of the models are complete. By a series of cooling runs the phase diagram is established. The map of the particle configuration, a result of the cooling run, formed a nonideal incommensurate phase. In the diffraction pattern of that configuration the intensities of the satellites, especially those of higher order, are considerably lower. The displacive system shows a soft, underdamped phonon mode, which with lowering temperature condenses at the critical wave vector, producing the incommensurate phase, in which the phase and amplitude modes are observed. The phase-mode dispersion curve does not show a gap. Adding 2% point defects to the system does not influence the phase and amplitude modes. The kinetics of the variation of the wave-vector modulation of the incommensurate phase has also been studied. The relevant nonequilibrium devil's staircase exhibits quasisteps at irrational numbers which are attributed to the nucleation and growth of new incommensurate periods observed as a stripple. Examples of nucleation inside and at the edges of the crystallite are given. Point defects hinder the propagation of the deperiodization line which borders the stripple.

I. INTRODUCTION

Incommensurate crystals, which are of great interest from both theoretical and experimental points of view, exhibit a superimposed periodic modulation in the atomic positions of the constituent atoms whose wave vector is generally incommensurate with the usual reciprocal-lattice wave vector. A number of simple models have been proposed for this behavior[1-3] with either the ground states of the models analyzed or the mean-field solution given. Much about incommensurate crystals is well understood, including the form of the incommensurate modulation and the related harmonic spectrum, the nature of the sinusoidal and soliton regimes, the discommensurations, the lock-in phases, the devil's-staircase behavior, the phase diagrams, and the peculiar elementary excitations of the incommensurate phase and also of the phase and amplitude modes. On the other hand, extensive experimental studies on a number of crystals such as Rb_2ZnBr_4,[4] thiourea,[5] tetramethylammonium-tetrachlorozincate (TMATC-Zn),[6] TMATC-Co,[7] quartz,[8] etc. by a number of precise experimental methods including x-ray and neutron diffraction, inelastic neutron scattering, Raman scattering, nuclear magnetic and quadrupole resonance, and dielectric and birefringence measurements, have led to results which can only be explained by processes more sophisticated than those studied in the models mentioned above. Various hysteresis effects[9,10], a memory effect,[11] an energy gap in the phase mode,[12,13] an unusual shape in the x-ray satellite reflections of an irradiated sample[7] and the intensities of higher harmonics (which can be orders of magnitude lower than those predicted by the mean-field approximation) also create problems. It is believed that these effects are associated with imperfections existing in the crystals, and such as fixed or mobile point defects, twin and grain boundaries, crystallite surfaces, or internal stresses, and may be related to the sometimes very slow kinetics of the incommensurate crystals. The complexity of the phenomena in imperfect incommensurate crystals makes their theoretical study fairly difficult. Therefore, a computer simulation of a model system of a considerable size in the incommensurate state could throw some light on the mechanisms of all those effects.

In this work we study a simple two-dimensional crystallite using the molecular-dynamics method. The method itself consists in iteratively solving the classical Newton equations of motion of all particles of the system. The particles of the model interact via a potential which, by changing some parameters, can reach a minimum for any desired wave vector k_p, but we are concerned with a one-dimensional incommensurate structure only. The crystallite can be heated or cooled to a given temperature and exhibits a phase transition to the incommensurate and/or commensurate phases. The results of the simulation are augmented by a direct observation of the particle configuration, including incommensurate modulation and stripples, and by the calculation of a conventional diffuse-scattering function $F(k)$ and dynamic structure factor $S(k,\omega)$.

Two very similar models, displacive and order-disorder in nature, have been studied. They differ in the characteristic relaxation times in which the system approaches equilibrium. The displacive model has a shorter, and the order-disorder model a longer relaxation time. We have also watched the effects of introducing 2% of substitutional point defects.

The outline of the paper is the following. In Sec. II we define the displacive and order-disorder models. In the next section we briefly discuss the Landau free-energy expansion and the ground-state energy. Then we construct the devil's staircase of the system at $T=0$. This is shown to be complete and to contain two strong lock-in phases at $k=0$ and $k=\frac{1}{4}$. The devil's staircase is the same for both models. Some details of the molecular dynamics method and the definitions of the diffuse scattering function and the dynamic structure factor are given in Sec. IV. Section V is devoted to the thermodynamic properties of the models. A sketch of the phase diagram and the phase-transition temperatures, as estimated by the molecular dynamics method, are also given. The incommensurate configuration of the ground state, reached by slow cooling to $T=0$, was far from perfect. The diffuse scattering function of such a configuration consisted of first-order satellites and sometimes of higher-order satellites. In Sec. VI. we study the elementary excitations of the displacive model for which we have found a soft phonon mode above the normal-incommensurate phase transition. Below T_c, gapless phase and amplitude modes are observed. Their frequencies agree with theoretical predictions. Surprisingly, the model doped with 2% point defects shows the same gapless phase- and amplitude-mode dispersion curves as those in the pure system. In Sec. VII, the kinetics of the variation of the satellite position of the nonequilibrium incommensurate phase caused by a continuous change in the potential-minimum wave vector k_p are studied. Such a curve can be called the nonequilibrium devil's staircase. The driving force of the mentioned process arises from the misfit between the wave vector k_p of the potential minimum and the characteristic wave vector of the current incommensurate phase. Except for the displacive model where this curve is partly continuous, an irregular steplike behavior is observed. The discontinuities in the gaps between the steps are caused by the nucleation and growth of new incommensurate periods. The nuclei of new periods is called a stripple. The stripple is formed from discommensuration planes which meet at one closed line called the deperiodization line. The steps of the nonequilibrium devil's staircase are not connected with rational numbers. Two runs, one with increasing, and the other with decreasing potential-minimum wave vector k_p, show the existence of global hysteresis. The nonequilibrium devil's staircase is not unique and depends on the initial conditions applied. The results allow one to conclude that defects hinder the growth and the propagation of deperiodization lines. Concluding remarks close the paper.

II. MODELS

The system is defined as a two-dimensional rectangular lattice with one particle per unit cell. Each particle can move out of the system plane and its displacement is $z_{n,m}$. The particles interact with each other via the following potential energy:

$$V=V^{(2)}+V^{(4)}\ , \tag{2.1}$$

where

$$\begin{aligned}V^{(2)}=\tfrac{1}{2}\sum_{n,m}[&A_0 z_{n,m}^2+A_1 z_{n,m}(z_{n,m+1}+z_{n,m-1})+A_2 z_{n,m}(z_{n,m+2}+z_{n,m-2})\\&+A_3 z_{n,m}(z_{n,m+3}+z_{n,m-3})+A_4 z_{n,m}(z_{n,m+4}+z_{n,m-4})+B_1 z_{n,m}(z_{n+1,m}+z_{n-1,m})\\&+B_2 z_{n,m}(z_{n+2,m}+z_{n-2,m})+C z_{n,m}(z_{n+1,m+1}+z_{n-1,m+1}+z_{n+1,m-1}+z_{n-1,m-1})]\ ,\end{aligned} \tag{2.2}$$

$$V^{(4)}=\tfrac{1}{2}G\sum_{n,m} z_{n,m}^4\ . \tag{2.3}$$

The constant G must be positive in order to stabilize the system.

To study the incommensurate phase one should choose such values of the model parameters that produce the incommensurate modulation. In practice, to find the appropriate parameters one should consider the quadratic form of the potential energy. Thus Eq. (2.2) can be transformed by

$$z_{n,m}=\sum_k Q(k)\exp[2\pi i(k_x na+k_y mb)] \tag{2.4}$$

into a diagonal form

$$V^{(2)}=\sum_k \omega^2(k)\,|\,Q(k)\,|^2\ , \tag{2.5}$$

where $k=(k_x,k_y)$ and

$$\begin{aligned}\omega^2(k)=&A_0+2A_1\cos(2\pi k_y b)+2A_2\cos(4\pi k_y b)+2A_3\cos(6\pi k_y b)+2A_4\cos(8\pi k_y b)+2B_1\cos(2\pi k_x a)\\&+2B_2\cos(4\pi k_x a)+2C\{\cos[2\pi(k_x a+k_y b)]+\cos[2\pi(k_x a-k_y b)]\}\ .\end{aligned} \tag{2.6}$$

In order to produce an incommensurate phase, the dispersion curve $\omega^2(k)$ should have its minimum at $k=k_p$. We intend to consider a one-dimensional modulation along the y direction, so we choose the minima of $\omega^2(k)$ along the [0,1] direction.

Temperature dependence in the wave-vector modulation has been observed in many incommensurate systems. This dependence is partly due to the temperature dependence of the minimum of the generalized soft mode and partly to the contribution from higher-order harmonics, coming into play below the transition temperature.[3] Since part of our interest is in the mechanism of the wave vector change of the incommensurate modulation, we assume that the minimum of $\omega^2(k)$ at k_p varies as a result of model-parameter changes. Below we shall study the processes which occur as a function of k_p, and shall keep the value of the minimum of $\omega^2(k_p)$ constant. Consequently, we assume that the two conditions $d\omega^2(k_p)/dk=0$ and $\omega^2(k_p)=\Omega$ specify the value of two parameters A_1 and A_2, the nearest- and next-nearest-neighbor harmonic force constants respectively. By varying A_1 and A_2 one can change the wave vector k_p. The remaining model parameters, which have been kept constant, are collected in Table I. The dispersion curves $\omega^2(k)$ for several k_p values along the incommensurate direction and those perpendicular to it are shown in Fig. 1.

Two models will be studied: a displacive model and an order-disorder one. The models differ in the local potentials,

$$V^{\rm loc}_{n,m}=A_0 z^2_{n,m}+G z^4_{n,m}\ , \tag{2.7}$$

only. In the displacive case ($A_0=2.0$) the local potential has one single minimum, in the order-disorder case ($A_0=-2.0$) it has two. The models differ in the relaxation times during which they approach the equilibrium. In a displacive case the relaxation is faster than in the order-disorder case. Both models possess only optic modes, so the elastic properties cannot be considered.

We have also studied models doped with 2% substitutional point defects. The defects are defined by another local potential. Namely, at the defect site the harmonic local force constant was $A_0=-10.0$ for both displacive and order-disorder models. All the other potential parameters of the defects were the same as for the host particles (Table I). Since the barrier between the two minima of the local potential at the defect site was rather high, the defect was almost always located in one of the minima. The distribution of defects, though random, was fixed. Therefore, diffusion was not permitted in the simulation.

III. LANDAU FREE ENERGY OF THE GROUND STATE

Consider the model as a classical system. Then the ground-state energy at zero temperature is given by the potential energy [(2.1)–(2.3)] in its ground-state configuration. Using Eq. (2.4) the potential energy can be transformed into the following form:

$$V/N=\tfrac{1}{2}\left[\sum_{kk'}\omega^2(k)Q(k)Q(k')\delta(k_x+k'_x-l_x a^*)\delta(k_y+k'_y-l_y b^*)\right.$$
$$\left.+G\sum_{k,k',k'',k'''}Q(k)Q(k')Q(k'')Q(k''')\delta(k_x+k'_x+k''_x+k'''_x-l'_x a^*)\delta(k_y+k'_x+k''_y+k'''_y-l'_y b^*)\right]\ , \tag{3.1}$$

where a^*b^* are the reciprocal vectors in the x and y directions, respectively, and l_x,l'_x, l_y, and l'_y are integers. Equation (3.1) contains normal ($l_x=l_y=l'_y=l'_y=0$) and Umklapp ($l_x,l_y,l'_x,l'_y\neq 0$) terms.

Our aim is to study the one-dimensional incommensurate modulation in the y direction. Hence without loss of generality we neglect the Umklapp terms in the y direction ($l_y=l'_y=0$). Let us decouple

$$Q(k)=\tfrac{1}{2}\sigma(k)\exp[-i\epsilon(k)]$$

from the amplitude $\sigma(k)$ and the phase $\epsilon(k)$.[3] Having counted the number of normal and Umklapp terms and confining the summation to only one harmonic characterized with the wave vector k_p we write down the ground-state energy per particle as[14,15]

TABLE I. Parameters of the displacive and order-disorder models, A_3, A_4, B_1, B_2, and C are the same in both models.

Displacive model parameters	Order-disorder model parameters	Parameters common to both models
$A_0=2.0$	$A_0=-2.0$	$A_3=-0.5$
$G=1000$	$G=2000$	$A_4=0.3$
$\Omega=-4.0$	$\Omega=-8.0$	$B_1=-1.5$
		$B_2=-0.1$
		$C=0.3$

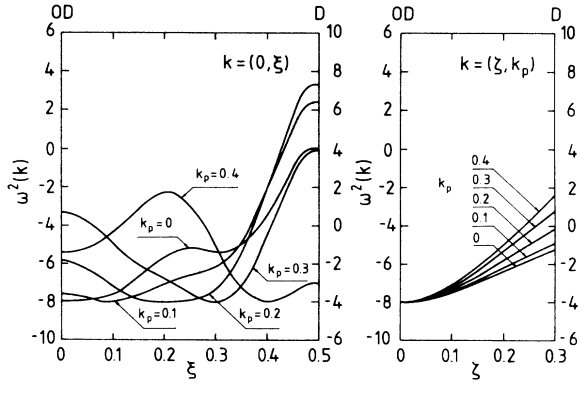

FIG. 1. Dispersion curves $\omega^2(k)$ for the displacive D and order-disorder (OD) models for several values of k_p. Left, $\omega^2(k)$ along the incommensurate direction y, right, $\omega^2(k)$ perpendicular to y and coming out from the minimum.

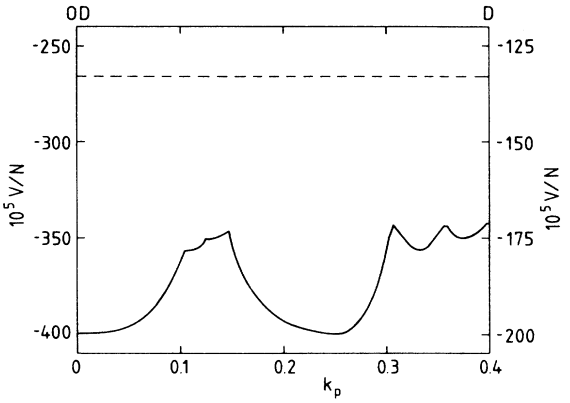

FIG. 2. Ground-state energy as a function of wave vector k_p for displacive D and order-disorder OD models.

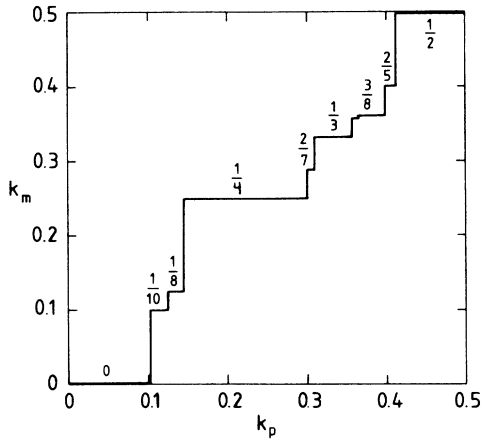

FIG. 3. The ground-state devil's staircase curve for displacive and order-disorder models.

$$V/N=\tfrac{1}{2}\{\tfrac{1}{2}\omega^2(k_p)\sigma^2(k_p)[1+\cos[2\epsilon(k_p)]\delta(2k_p-l_xa^*)] + \tfrac{1}{8}G\sigma^4(k_p)[3+4\cos[2\epsilon(k_p)]\delta(2k_p-l_xa^*)+\cos[4\epsilon(k_p)]\delta(4k_p-l_xa^*)]\} \ . \tag{3.2}$$

For strong commensurate phases, and at the minimum with respect to the phase $\epsilon(k)$, one finds

$$k_p=0 \text{ phase: } V/N=\tfrac{1}{2}[\omega^2(0)\sigma^2(0)+G\sigma^4(0)] \ , \tag{3.3}$$

$$k_p=\tfrac{1}{2} \text{ phase: } V/N=\tfrac{1}{2}[\omega^2(\tfrac{1}{2})\sigma^2(\tfrac{1}{2})+G\sigma^4(\tfrac{1}{2})] \ , \tag{3.4}$$

$$k_p=\tfrac{1}{4} \text{ phase: } V/M=\tfrac{1}{2}[\tfrac{1}{2}\omega^2(\tfrac{1}{4})\sigma^2(\tfrac{1}{4})+\tfrac{1}{4}G\sigma^4(\tfrac{1}{4})] \ , \tag{3.5}$$

and additionally the phases $\epsilon(0)=\epsilon(\frac{1}{2})=0,\pi$ and $\epsilon(\frac{1}{4})=\pi/4,3\pi/4,\ 5\pi/4,\ 7\pi/4$. Setting for the displacive model $\omega^2(0)=\omega^2(\frac{1}{2})=\omega^2(\frac{1}{4})=-4.0$ and $G=1000$ and using the condition of the minimum with respect to the amplitude of the order parameter, we get $V/N=-0.002$ for $k_p=0$, $\frac{1}{2}$, and $\frac{1}{4}$.

For illustration we write down the ground-state energy of a sinusoidal modulation given by the first harmonic only

$$V/N=\tfrac{1}{2}[\tfrac{1}{2}\omega^2(k_p)\sigma^2(k_p)+\tfrac{3}{8}G\sigma^4(k_p)] \ . \tag{3.6}$$

Setting $\omega^2(k_p)=-4.0$ for all k_p and $G=1000$ one finds for the displacive model with sinusoidal modulation $V/N=-0.001\,33$. As it is shown presently contributions from higher order harmonics bring this energy much below that value.

The modulation in the model is certainly accompanied by higher-order harmonics.[14,15] The fourth-order Umklapp terms (1,3,3,3), (1,1,3,3), (1,1,1,3), and (3,3,9,9) between the first and the third-order harmonics are responsible for the lock-in phases $\frac{1}{10}$, $\frac{1}{8}$, $\frac{1}{3}$, and $\frac{3}{8}$, respectively.

The ground-state energy for the one-dimensional modulation in the y direction was also found numerically. For that a linear chain in the y direction of the M-particle model with periodic boundary conditions was used. The force constants A_1 and A_2 were set so that the potential energy had a minimum at the desired wave vector k_p. The initial configuration was chosen in the form of a sinusoidal modulation characterized by a commensurate wave vector $k_m=M'/M$, where M' and M are integers. The ground-state energy is given by the minimum of $V/N=f(k_m,k_p)$ as a function of k_m and fixed k_p. To calculate it we searched for the minimum of the potential energy, Eqs. (2.1)–(2.3), with a fixed k_p and with respect to wave vector k_m. The calculations for the present model were performed by the numerical method described in Ref. 3. The results for the displacive and order-disorder models are shown in Fig. 2. Each point in the V/N curve corresponds to a lock-in phase. It is worth mentioning that in spite of a constant $\omega^2(k_p)=\Omega$ and constant G values for all wave vectors k_p, the ground-state energy varies remarkably.

The relation $k_m=g(k_p)$ between the two wave vectors at the minimum of the potential $V/N=f(k_m,k_p)$ can be called the devils' staircase of the ground state[16] and the results of our model calculations are presented in Fig. 3. One notices there large lock-in steps for 0, $\frac{1}{4}$, and $\frac{1}{2}$, and smaller ones for $\frac{1}{10}$, $\frac{1}{8}$, $\frac{2}{7}$, $\frac{1}{3}$, $\frac{3}{8}$, and $\frac{2}{5}$. The ground state devil's staircase is complete.

IV. THE MOLECULAR-DYNAMICS METHOD

The system used in the simulation was a two-dimensional crystallite consisting of 97×97 rectangular unit cells with one particle per unit cell. The use of free boundary conditions allowed the nodes of the incommensurate phase and extended detects, like stripples, to flow out of the system. The Newton equations of motion for

all 9409 particles were solved by a simple difference scheme using the microcanonical ensemble with total energy conserved. The iteration step was $\Delta t=0.05\tau_0$, where $\tau_0=2\pi/\omega_0$ was our time unit and $\omega_0=1$ is a unit in Fig. 1. The temperature was described by average kinetic energy. Each run of calculations started from random initial velocities and positions and the system was always allowed to equilibrate. The system can be cooled or heated by delicate changes of particle velocities in each iteration step. Moreover, by continuously changing force constants A_1 and A_2 the minimum of the potential at the wave vector k_p can be altered. The last process does not conserve the energy of the system any longer. For further details of the method itself see Ref. 17.

The results of the simulation have been elaborated in the following ways. First, in the form of a map of average particle displacements $\langle z_{n,m}\rangle_\tau$, where τ denotes the averaging time. The two kinds of symbols on the maps correspond to positive and negative displacement of $\langle z_{n,m}\rangle_\tau$, respectively. The size of the symbol is proportional to the amplitude of $\langle z_{n,m}\rangle_\tau$.

Second, the incommensurate modulation has been detected due to the existence of the diffraction satellites. For this purpose we have calculated the diffuse scattering function defined as a time average of the time-independent correlation function

$$F(k)=\langle\chi^*(k,t)\chi(k,t)\rangle_\tau . \tag{4.1}$$

The Fourier transform of particle density of the crystallite is given by

$$\chi(k,t)=\frac{1}{N}\sum_{n,m}\exp\{-2\pi i[kR_{n,m}+|k|z_{n,m}(t)]\}Q_{n,m} , \tag{4.2}$$

where

$$Q_{n,m}=\exp(-\lambda R_{n,m}^2) \tag{4.3}$$

is a space damping factor, $R_{n,m}$ is the position of particle n,m, and $R_{n,m}=0$ corresponds to the center of the crystallite. The lattice constant is taken as a unity and λ was chosen to be equal to 0.0002. The factor (4.3) involves a finite wave vector resolution and makes possible calculating the quantities for any wave vector k, unlike the periodic boundary conditions method without $Q_{n,m}$, which would allow one to find quantities at discrete wavevectors. A typical time average in the correlation function, Eq. (4.1), was $125\tau_0$. The diffuse-scattering function contains the Bragg reflections and usually not intense satellites. Thus, for practical reasons, it is better to decouple Eq. (4.2) into

$$\chi(k,t)=\langle\chi(k,t)\rangle_\tau+\mu(k,t) \tag{4.4}$$

and calculate the two terms separately. Then

$$F(k)=|\langle\chi(k,t)\rangle_\tau|^2+\langle\mu^*(k,t)\mu(k,t)\rangle_\tau . \tag{4.5}$$

The first term describes the Bragg reflections occurring at the Γ points, the second one the diffuse scattering.

Third, to study the elementary excitations one should calculate the dynamical structure factor which is defined by the time-dependent correlation functions as

$$S(k,\omega)=\frac{1}{2\pi}\int_{-\infty}^{\infty}dt\langle\chi^*(k,0)\chi(k,t)\rangle_\tau \times\exp\left[-\left[\frac{t}{\nu}\right]^2\right]\exp(i\omega t) , \tag{4.6}$$

where $\chi(k,t)$ is given by Eq. (4.2). We have included in the transformation the Gaussian damping factor. The "experimental" energy resolution in $S(k,\omega)$ is $\Delta\omega=(4/\nu)(\ln 2)^{1/2}$. By applying Eq. (4.4) the dynamical structure factor can be decoupled into elastic and inelastic parts

$$S(k,\omega)=S^{\rm el}(k,\omega)+S^{\rm ie}(k,\omega) , \tag{4.7}$$

where

$$S^{\rm el}(k,\omega)=\langle\chi^*(k,0)\rangle_\tau\langle\chi(k,t)\rangle_\tau\frac{\nu}{2\pi}\exp[-(\nu^2\omega^2)/4] \tag{4.8}$$

and

$$S^{\rm ie}(k,\omega)=\frac{1}{2\pi}\int_{-\infty}^{\infty}dt\langle\mu^*(k,0)\mu(k,t)\rangle_\tau \times\exp\left[-\left[\frac{t}{\nu}\right]^2\right]\exp(i\omega t) . \tag{4.9}$$

Below the analysis of the excitations has been made with the aid of the inelastic part of the dynamical structure factor Eq. (4.9) with the averaging time $1000\tau_0$.

V. STATIC PROPERTIES OF THE MODELS

Let us first look at the particle configuration at $T=0$. For this the following run with the order-disorder model has been performed. The wave vector k_p was fixed. The system was cooled from the normal phase to zero temperature. The cooling rate was $dT/dt=-0.000\,03(1/\tau_0)$. The resulting incommensurate modulations, Fig. 4, are nonperfect. Although the existence of the incommensurate structure is evident, the nodes of the modulation do not form a straight line perpendicular to the modulation, but an irregular front. Figure 4 shows two such examples: for $k_p=0.10$ and for $k_p=0.11$. The relevant diffuse scattering functions, Fig. 5, contain first-order satellites. The intensity of these satellites is higher for $k_p=0.10$ than for $k_p=0.11$.

The deviation of the configurations from an ideal structure can be described either by a set of subharmonics or by frozen phase modes and the effect should be taken into account in the structural analysis of incommensurate phases. In some cases, especially when the system is of highly order-disorder type, the incommensurate phase might not reach true equilibrium state and then the ratio of higher-order satellite intensities to the first-order satellite intensity might turn out to be too small in comparison with the predictions of the mean-field theory, which assumes the equilibrium state.

The molecular-dynamics method allows one to also study the evolution of the system as a function of temperature. For that, we have slowly cooled the system

from normal phase with cooling rate $dT/dt = -2\times10^{-7}(1/\tau_0)$ leaving the wave vector k_p fixed and registering the position of the satellites. For the displacive model the results of nine such runs are presented in Fig. 6. The transition temperature T_c is defined to be at the point at which the satellite appears for the first time. The incommensurate phases obtained for the wave vectors k_p, which are far from strong commensurate phases 0 and $\frac{1}{4}$, have the satellite position $k_m = k_p$. The phases characterized by $k_p = 0.20$ and $k_p = 0.275$ behave differently.

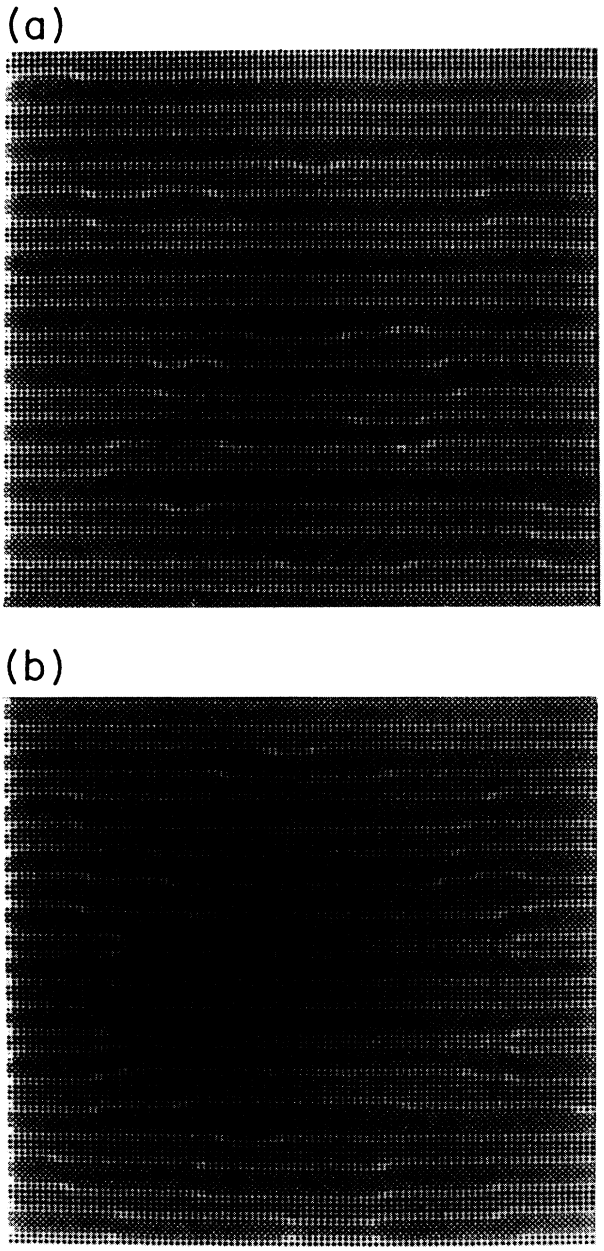

FIG. 4. Configuration of particles of an order-disorder model at $T=0$ for (a) $k_p=0.10$ and (b) $k_p=0.11$.

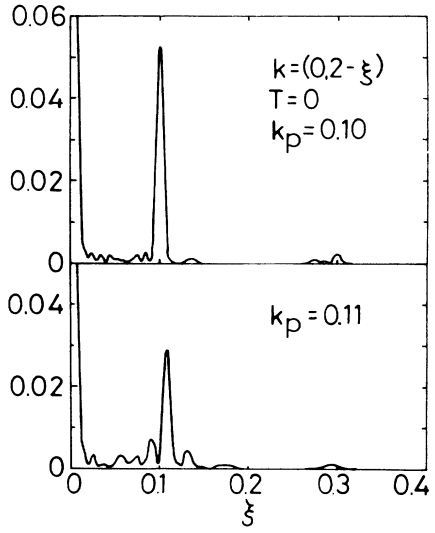

FIG. 5. Diffuse-scattering functions of an order-disorder model at $T=0$ for $k_p=0.10$ and $k_p=0.11$ which correspond to two maps in Fig. 4.

Just below T_c the satellite occurs at k_p. Then, during cooling, its position k_m shifts to the lock-in value $\frac{1}{4}$, but the structure contains a lot of defects and the satellite itself is split and not well defined. At the end of the cooling run the phase $\frac{1}{4}$ contains several domains. For $k_p=0.175$, we have obtained a coexistence of two phases, one with modulation $k_p=0.15$ and the other with $k_p=0.25$.

According to our ground-state devil's staircase, Fig. 3, the wave vectors k_p of the runs with $k_p=0.15$, 0.30 and 0.35 should have been locked at commensurate phases $\frac{1}{4}$, $\frac{2}{7}$, and $\frac{1}{3}$, respectively. That did not happen, since the driving forces of these lock-in phases were too small and the cooling rates were in any case too fast to achieve a

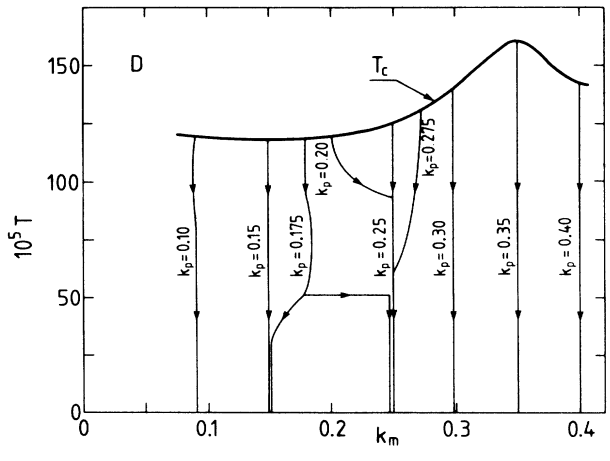

FIG. 6. Phase diagram and phase-transition temperature T_c of the displacive model for several values of the wavevector potential minimum k_p constructed from the cooling runs.

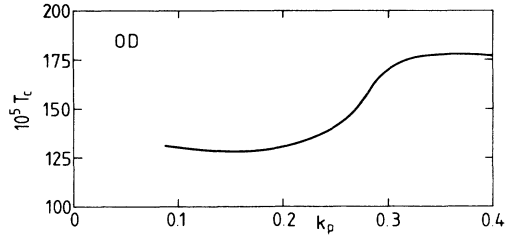

FIG. 7. Transition temperature T_c of the order-disorder model constructed from the cooling runs.

true equilibrium.

In the order-disorder model the characteristic relaxation times were so long that in our computer simulation only the transition temperature T_c from the normal to the incommensurate phase could be estimated, Fig. 7. The temperature behavior of the satellite position would need cooling rates unavailable in the simulation.

VI. EXCITATIONS IN THE DISPLACIVE MODELS

The elementary excitations were studied for the pure displacive model and for the displacive model doped with 2% of point defects. Before searching for the excitations the system, with a fixed value of wave vector k_p, was equilibrated at a desired temperature. The frequency spectrum was calculated using the inelastic dynamical structure factor Eq. (4.9). The positions of the peaks of several runs are collected in Figs. 8 and 9. The error bars there denote the widths of the peaks at half maximum.

In the displacive model above T_c the observed phonons are underdamped. The form of the phonon dispersion curve in Fig. 8 resembles the bare dispersion curve, Eq. (2.6), for $k_p=0.35$. The squared frequency $\omega_s^2(k_p)$ at its minimum as a function of temperature is shown in the lower drawing of Fig. 8. The $\omega_s^2(k_p)$ behaves as a typical soft mode and from our numerical simulation its temperature dependence can be approximated by

$$\omega_s^2(k)=\omega^2(k)-\Omega+\beta(T-T_c) \tag{6.1}$$

where $\Omega=-4.0$, $\beta=480$, and one has $\omega_s^2(k_p)=0$ at $T_c=0.00161$. The $\omega^2(k)$ is given by Eq. (2.6).

In the displacive model the excitations below T_c and those in the incommensurate phase are referred to as the phase mode and the amplitude mode, respectively. The dynamical structure factor calculated at $T=0.00088$ for

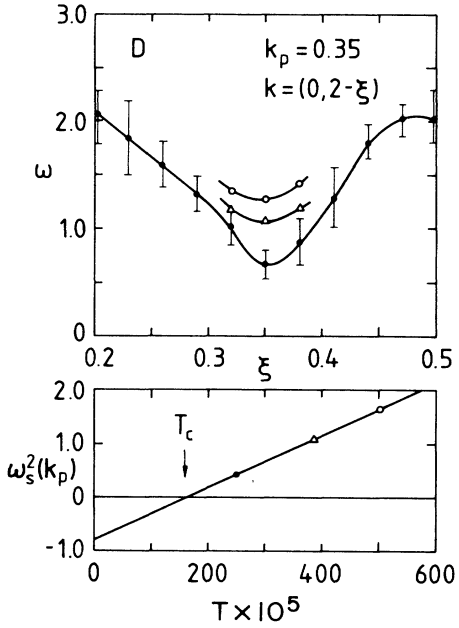

FIG. 8. (Upper) Phonon dispersion curves of the displacive model at $T=0.00248$ (●), $T=0.00373$ (△), and $T=0.00502$ (○), above T_c. (Lower) Temperature behavior of the soft mode. Lines are guides to the eyes.

pure and doped systems with $k_p=0.35$ showed well-defined peaks whose positions are given in Fig. 9. Figures on the left-hand side present the dispersion curves along the incommensurate modulation, right depict those perpendicular to it. At some wave vectors separate peaks for the phase and amplitude modes were observed. Within the accuracy of the simulation, the phase mode remains gapless in both cases.

The relation between the soft mode dispersion above T_c and the phase and amplitude modes below T_c has been derived, for example, by Bernard *et al.*[18] Following their approach we start from the free energy in the form similar to Eq. (3.1), where the bare dispersion curve $\omega^2(k)$ has been replaced by the effective soft mode $\omega_s^2(k)$ and all Umklapp terms have been neglected. Assuming further the sinusoidally modulated structure, we arrive at the following result for the phase and amplitude modes:

$$\omega_{\mathrm{ph,am}}^2(k_p+q)=\tfrac{1}{2}(\omega_s^2(k_p+q)+\omega_s^2[(k_p-q)-4\omega_s^2(k_p)\pm\{4\omega_s^4(k_p)+[\omega_s^2(k_p+q)-\omega_s^2(k_p-q)]^2\}^{1/2}) . \tag{6.2}$$

Since the soft-mode behavior is known, Eq. (6.1), the formula (6.2) does not leave free parameters. The continuous curves in Fig. 9 have been calculated with the help of Eqs. (6.2) and (6.1) using displacive model parameters from Table I. In both cases the agreement is quite good. It is worth mentioning that mistaking the phase mode for an acoustic phonon mode, a severe experimental problem, cannot occur here, since our model does not have an acoustic mode at all.

In spite of a rather high concentration of defects, the dispersion curve of a doped model looks the same as that for the pure system. Even the intensities and widths of the inelastic peaks have not been affected by the defects. This astonishing result has the following origin. The sys-

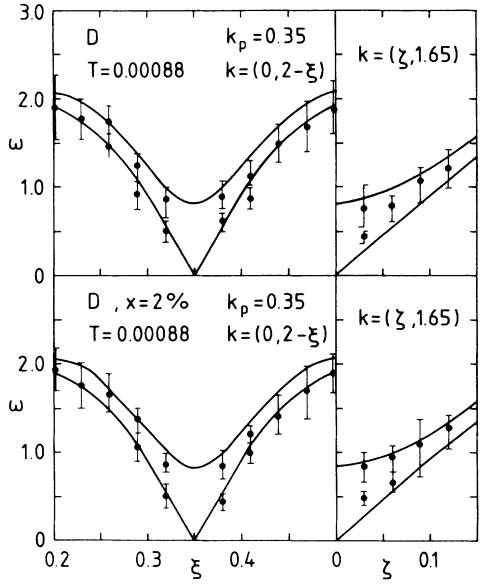

FIG. 9. Phase and amplitude-mode dispersion curves for the displacive model and the displacive model with 2% point defects. The lines are calculated from Eq. (6.2).

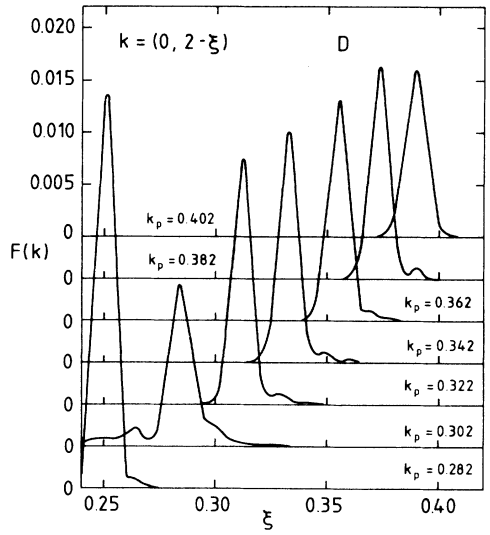

FIG. 10. Satellite behavior of the displacive model during the kinetic run as a function of the wave vector k_p which changes from 0.28 to 0.40. Points on Fig. 11 indicate the positions of maxima of these satellites.

tem is in a state closer to the soliton limit. In this limit the phase mode corresponds to oscillations in the soliton position and the defects, sitting in one of the local potential minima but interacting with neighbors via the same forces as the host particles, also take part in the soliton motion. In this sense the defects do not perturb the motion much. Similar runs performed for the commensurate phase $k_p=\frac{1}{4}$ at $T=0.000\,84$ revealed, as expected, a large gap for the observed dispersion curve.

VII. KINETIC BEHAVIOR OF THE INCOMMENSURATE MODULATION

As a rule, the characteristic wave vector of the incommensurate structure varies with changing the temperature. Two incommensurate modulations, $k_m^{(1)}$ and $k_m^{(2)}$, of the same sample at two temperatures characterize different phases of the crystal. Formally, according to the Landau theory of phase transitions, the two incommensurate phases $k_m^{(1)}$ and $k_m^{(2)}$ arise as a result of the condensation of two different irreducible representations of the high-symmetry space group. The two representations are different, because they belong to two different wave vectors. Let us assign a supergroup to each of the phases. Because of a difference in the translational symmetry elements, the group-subgroup relationship between these supergroups does not exist. Therefore, the phase change from the modulation $k_m^{(1)}$ to $k_m^{(2)}$ must be governed by the mechanism similar to that characteristic for the first-order phase transitions. Then the order parameter is not a normal mode but a local perturbation in the form of special dislocation.

In real incommensurate systems the minimum at k_p of the generalized soft mode $\omega_s^2(k)$ often shifts as a function of temperature, because of its renormalization by fluctua-

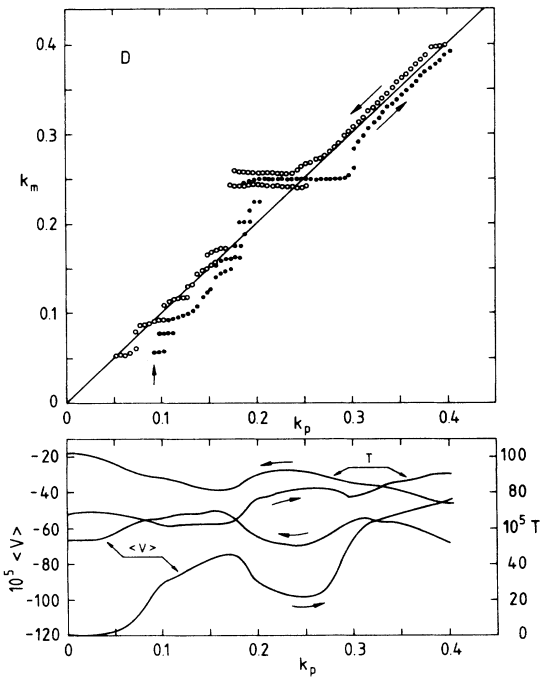

FIG. 11. Position of diffraction satellites in the displacive model detected by the diffuse scattering function $F(k)$ as a function of the wave vector k_p for a constant rate $dk_p/dt=\pm 4\times 10^{-5}(1/\tau_c)$. Closed and open points correspond to 0.0→0.4 and 0.4→0.0 runs, respectively. In the lower part the variation of T temperature and $\langle V\rangle$ the average potential energy during the runs are given.

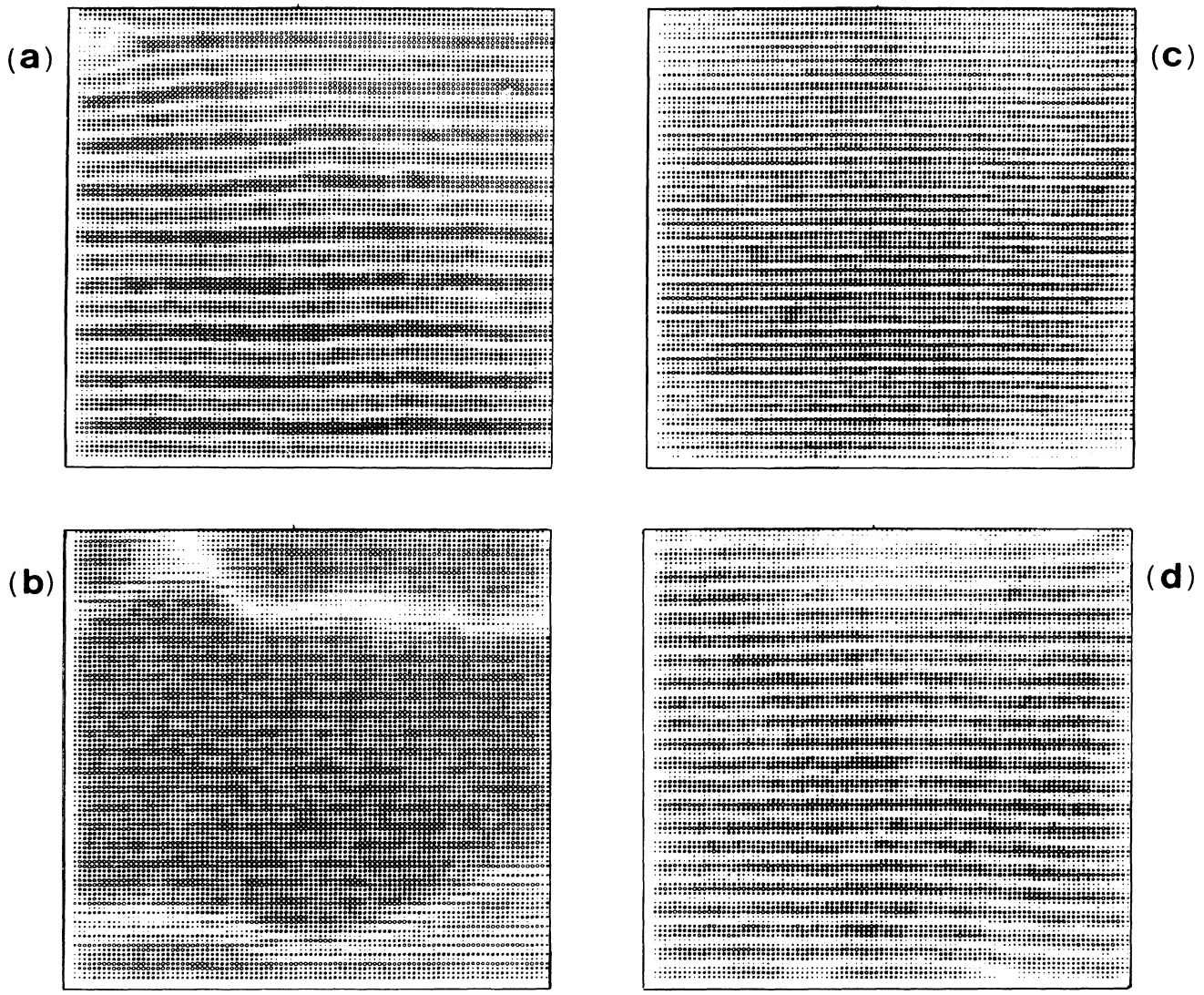

FIG. 12. Configuration of particles in the increasing run $k_p = 0.0 \rightarrow 0.4$, for the wave vectors $k_p = 0.12$, 0.20, 0.30, and 0.40, maps (a), (b), (c), and (d), respectively.

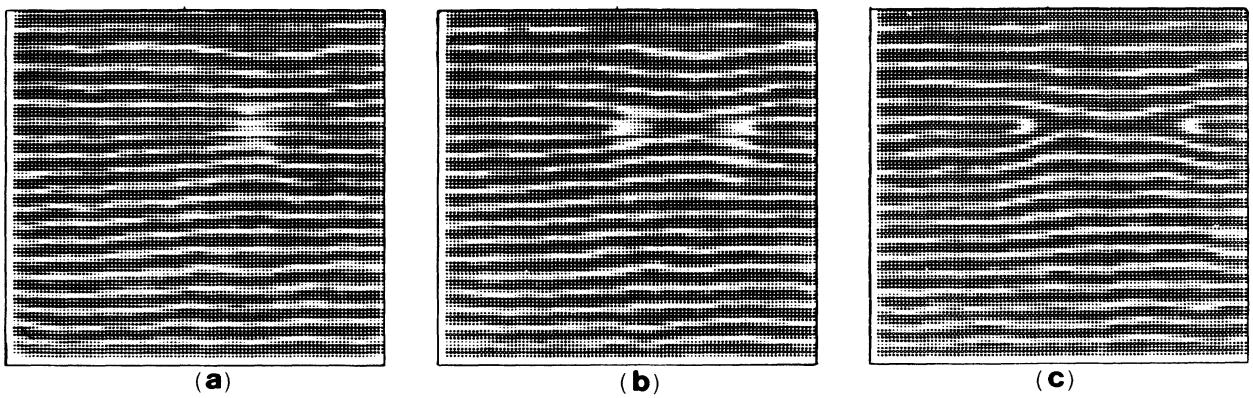

FIG. 13. Example of homogeneous nucleation and growth of the extra period of incommensurate modulation. The maps (a), (b), and (c) correspond to $k_p = 0.375$, 0.385, and 0.395, respectively.

tions of other modes. So, in experiment one may influence the position of the minimum at k_p only by varying the temperature, the pressure or the external field applied to the sample. In order to study in computer simulation the mentioned mechanisms we have introduced the following simplification. We shift the minimum of $\omega^2(k)$, keeping $\omega^2(k_p)$ constant at its minimum, by varying in time the force constants A_1 and A_2 of the potential energy. That approach simulates the renormalization of $\omega^2(k)$ by fluctuation of other modes, not existing in our models. Thus below, we study the behavior of our crystallite varying in time its potential energy so that the wave vector k_p of the minimum of $\omega^2(k)$ changes in time with a constant rate.

Two kinds of independent runs were studied, an increasing one from $k_p=0$ to 0.4 and a decreasing one from $k_p=0.4$ to 0. Each run started from an equilibrium configuration which was either a one-domain phase with $k_p=0$ or a phase $k_p=2/5$. Then k_p was changed at a constant rate $dk_p/dt=\pm 4\times 10^{-5}(1/\tau_0)$ and during that process the diffuse-scattering function $F(k)$, Eq. (4.1), was calculated. The $F(k)$ was sampled only on the line from (0, 2.0) to (0, 1.6) in reciprocal space. Each point of $F(k)$ was a result of a time average over $125\tau_0$ while the whole run from $k_p=0$ to 0.4 or the reverse lasted $10^4\tau_0$. During this kinetic process energy is inserted into the system, so the temperature rose. Therefore, we made sure that the starting temperature was sufficiently low for the system to remain in the incommensurate state at the end of the run.

A. Displacive model

An example of the shape and intensity variations of the satellites calculated by $F(k)$ as a function of a continuous change of wave vector k_p is shown in Fig. 10. Figure 11

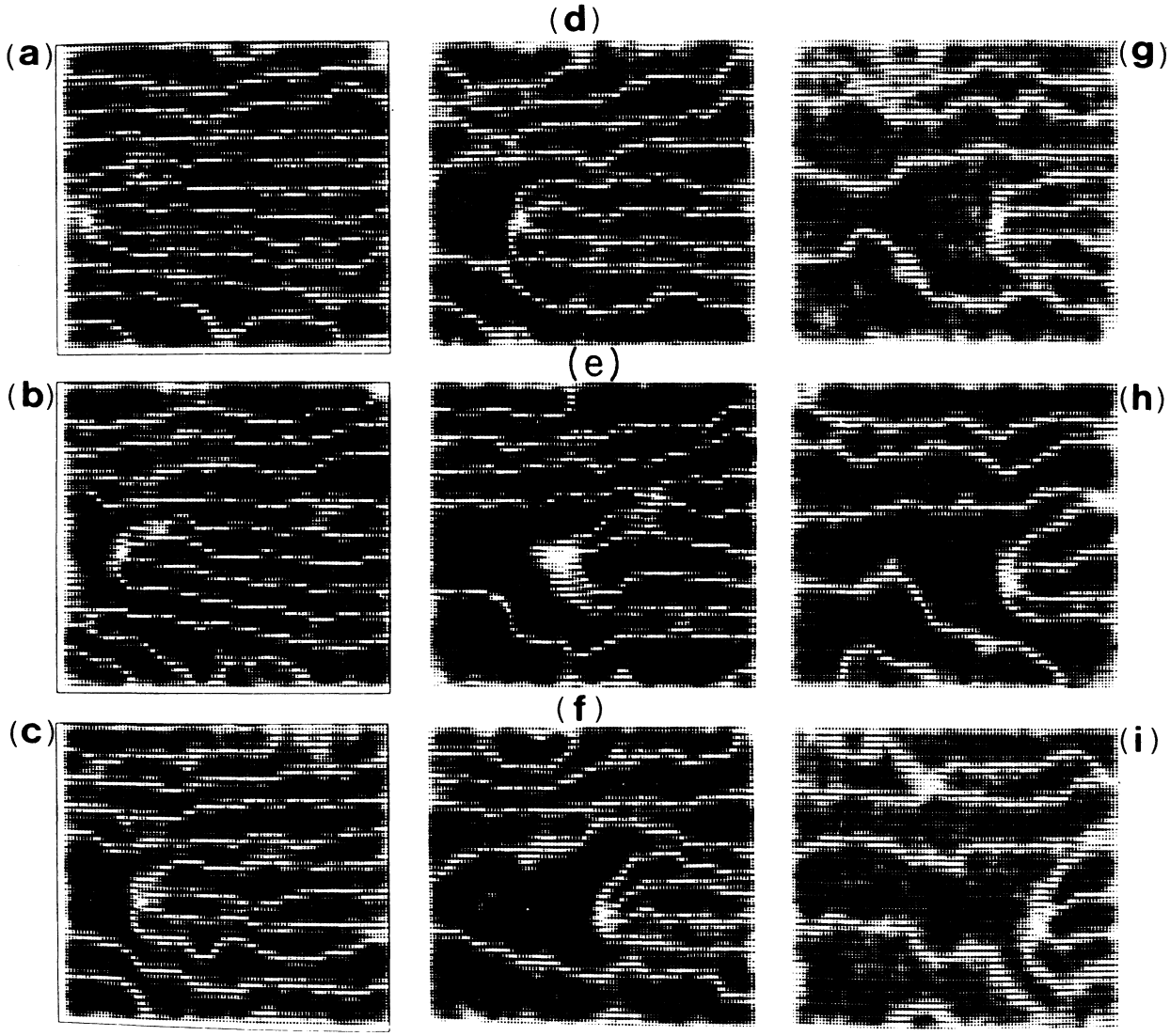

FIG. 14. Subsequent configuration maps in the process where the k_p changes from 0.2744 [map (a)] to 0.2616 [map (i)]. The duration of the process is $320\tau_0$.

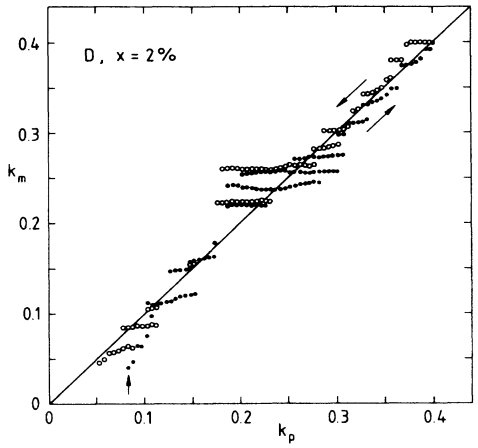

FIG. 15. Position of diffraction satellites in the displacive model with 2% of point detected by the diffuse scattering function $F(k)$ as a function of the wave vector k_p for a constant rate $dk_p/dt = \pm 4\times 10^{-5}(1/\tau_0)$. Closed and open points correspond to $0.0\rightarrow 0.4$ and $0.4\rightarrow 0.0$ runs, respectively.

shows the position of the maximum of the satellites as a function of the wave vector k_p for the increasing and decreasing runs of k_p. The points in Fig. 11 characterize the configurations which, except for the initial one, do not necessarily correspond to the equilibrium state and therefore, they define the nonequilibrium devil's staircases.

The relaxation toward equilibrium in the range of $k_p = 0.27$–0.40 is so fast that the satellite position changes continuously. In the vicinity of $k_p = 0.25$, the modulation locks into the commensurate phase $k_p = \frac{1}{4}$. The observed splitting of the satellite is due to the domain structure of the phase at $k_p = \frac{1}{4}$. Below $k_p < 0.18$ an irregular variation of the satellite position with a two- or three-peak structure sometimes occurs. At $k_p \sim 0$, one observes the commensurate $k_p = 0$ phase in a few domain state. The satellite of this phase emerges into the Bragg peak and thus it cannot be separated out. Global hysteresis between increasing and decreasing runs, and especially around the lock-in phase $\frac{1}{4}$, is clearly seen.

In Fig. 11 we also give temperature T and the average potential energy $\langle V \rangle$ variation along the runs. The potential energy resembles the ground-state energy curve from Fig. 2.

Figure 12 presents a map of the average configuration of particles for a few values of k_p of the increasing run shown in Fig. 10. On each map the positions averaged over a time of $125\tau_0$ are drawn. On maps with the wave vector modulation $k_p < \frac{1}{4}$, the white strips of small average displacements $\langle z_{n,m} \rangle_\tau$ correspond to the nodes of incommensurate modulations. In the remaining cases, $k_p > \frac{1}{4}$, the white lines describe the discommensurate regions. One notices that the fronts of the incommensurate modulations are not straight horizontal lines, as could be expected for the ideal incommensurate structure. The phase at $k_p = 0.20$ consists of several lock-in domains $\frac{1}{4}$, which causes the splitting of the satellite.

Beside the lock-in phases $\frac{1}{4}$ and 0, no other commensurate phases have been detected, because the lock-in energies of these unobserved commensurate phases were too small, the temperature of the runs too high and the rated dk_p/dt too fast to allow good equilibration.

An analysis of many pictures of particle configurations allows one to draw conclusions about the mechanism of the change of the incommensurate wave vector. The driving force of this process results from a misfit between the wave vector k_p and a characteristic wave vector of a current structure. Simple mechanisms have been observed. In one an extra period is inserted or removed at the top or bottom of the crystallite by a kink traveling along the top or bottom edge of the system. Such a situation occurs on the map in Fig. 12(d) for the wave vector $k_p = 0.40$. One sees there that the discommensuration line leaves the crystallite not at the right edge but at the bottom. In the course of time this anomalous part of the discommensuration moves horizontally from left to right adding one period of modulation. In another mechanism an extra period is inserted in the form of a half-stripple at the left or right edge of the crystallite. In three dimensions the stripple is a nucleus formed from additional discommensuration planes which fit to the surrounding incommensurate modulation and which meet along one closed line called the deperiodization line.[19,20] After spontaneous nucleation the stripple grows by the propagation of the deperiodization line which eventually comes to the surface. In our maps the deperiodization line is seen as a white spot. Example of initial stage of the half-stripple is given in the left upper corner of Fig. 12(a) for the wave vector 0.12. The third mechanism consists in the homogeneous nucleation of a stripple within the crystallite and afterwards in the growth of it. Figure 13 illustrates the stages of this process. The antistripple arises as a result of accidental concentration of energy fluctuation and can be noticed in Fig. 13(a). Later it grows to the left and to the right, Figs. 13(b) and 13(c), by motion of the deperiodization line.

An example of a more complicated mechanism is presented on Fig. 14. The maps show the subsequent configurations in the process of decreasing the wave vector k_p and close to the commensurate phase $\frac{1}{4}$. The stripes on the map (a) correspond to discommensuration lines which in this case are the domain walls between regions of commensuration phase $\frac{1}{4}$. The stripple, related with the commensurate phase $\frac{1}{4}$, consists of at least four discommensuration planes which confine regions belonging to three different domains of phase $\frac{1}{4}$. Indeed, if the surrounding commensurate domain is characterized by the phase $\epsilon(\frac{1}{4}) = \pi/4$ then the domains within the stripple must form a sequence of domains with phases $\epsilon(\frac{1}{4}) = 3\pi/4$, $5\pi/4$, and $7\pi/4$. Other sequences would cost too much energy. On the map (b) a half-antistripple, seen as a bundle of four discommensuration lines which meet in the deperiodization point, split out from the left middle edge of the crystallite and on the (c) to (i) maps it moves toward the right edge leaving behind a large region of commensurate phase $\frac{1}{4}$.

The above results largely resemble the electron micrographs obtained by Fung *et al.*[21] for charge-density wave bearing material 2H-$TaSe_2$ and serve a good illustration to

the theoretical predictions by Kawasaki,[20] Prelovsek and Rice,[22] and Janovec.[19]

B. Displacive model with 2% of point defects

Figure 15 shows the position of the maxima of the satellites in increasing and decreasing runs or in other words the nonequilibrium devil's staircases for displacive model with 2% of point defects. The previously observed continuous behavior in the range of $k_p = 0.28$—0.40, Fig. 11, has disappeared. Now quasisteps tend to be seen. In the $\frac{1}{4}$ phase, few domains remain in the crystallite throughout the whole range of stability, producing splitting of the satellites. The global hysteresis is again present. The essential result of these calculations is that the continuous change of the satellite positions is now replaced by a rather steplike behavior and these steps cannot be related to any rational numbers except for the strongest lock-in phase, $k_p = \frac{1}{4}$. The intensities of the satellites of the system with defects are considerably lower than those for the pure cases. This is a consequence of the highly imperfect and defective incommensurate modulation.

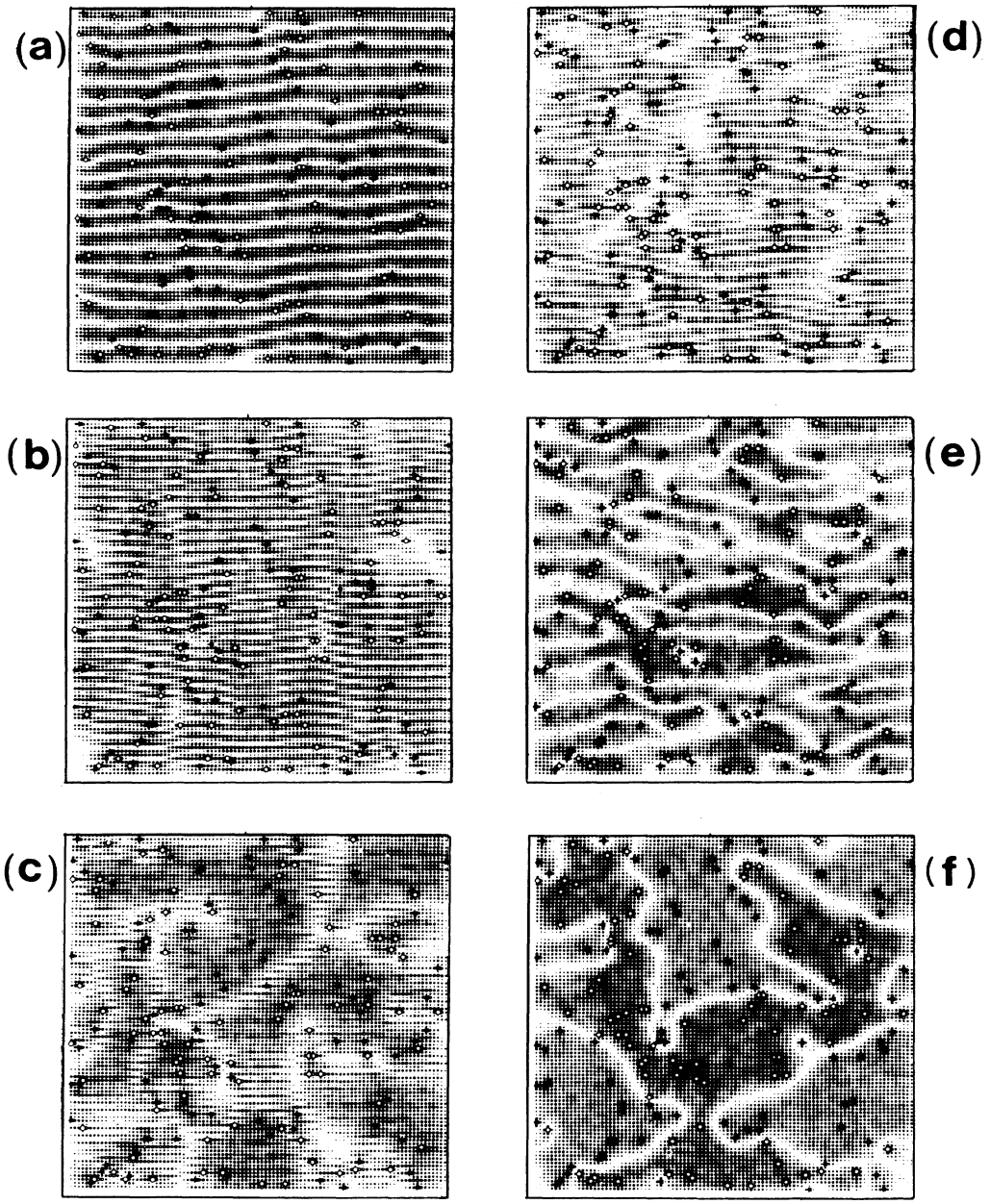

FIG. 16. Configuration of particles in the decreasing run $k_p = 0.4 \rightarrow 0.0$, for the wave vectors $k_p = 0.395$, 0.315, 0.235, 0.155, 0.075, and 0.005, maps (a)—(f), respectively, and for the displacive model with 2% of point defects.

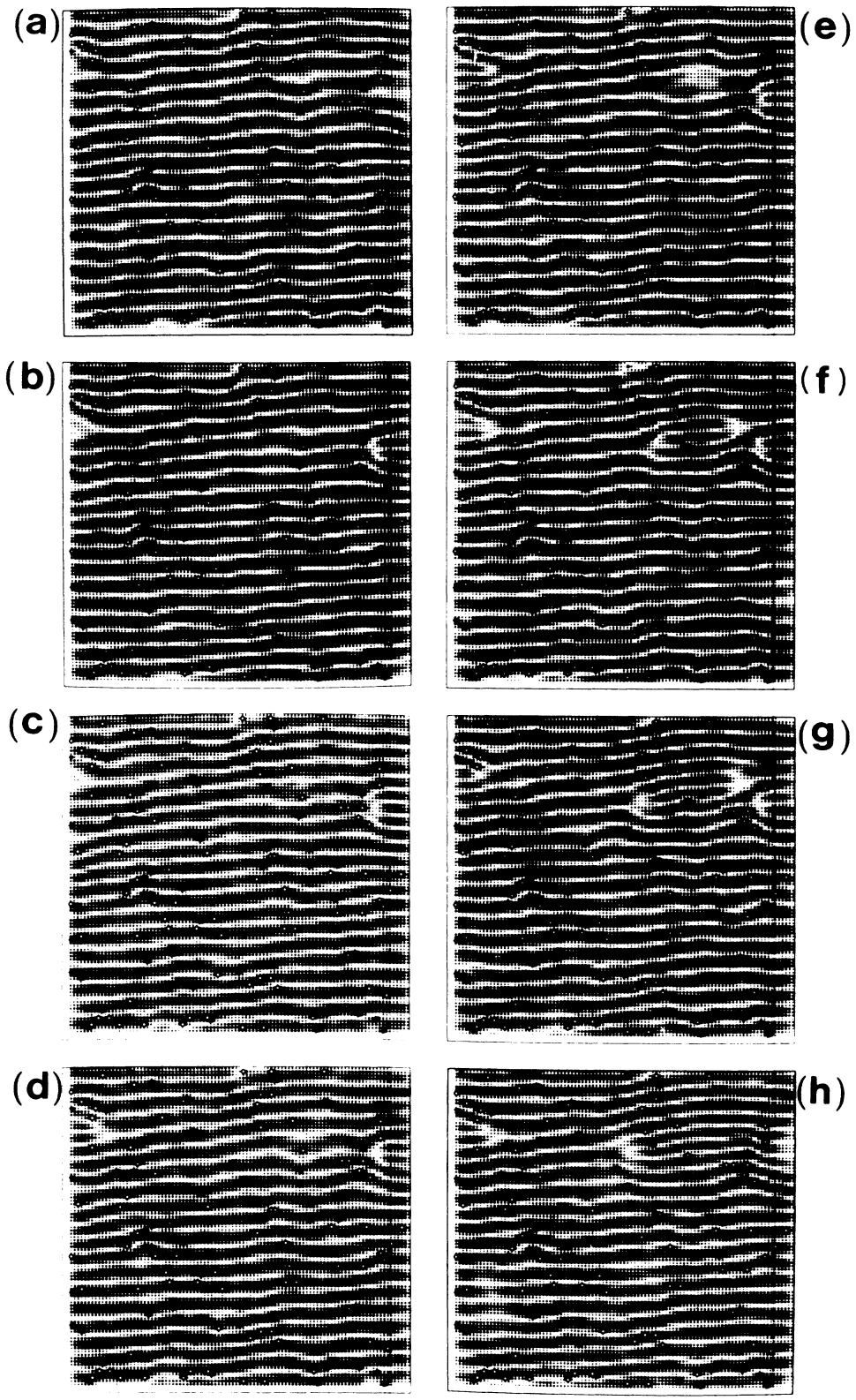

FIG. 17. Example of the propagation of the extra incommensurate period in the displacive model with 2% of defects. The wave vector from (a) to (h) changes from 0.3672 to 0.3792 during $200\tau_0$.

In Fig. 16 a few maps of a decreasing run are shown. During the equilibration of the starting configuration at $k_p = 0.40$ the defects were trapped in one of the minimum of their local potential and this local minimum was occupied which agreed with the displacements of the incommensurate modulation at a given location. During the run the incommensurate modulation tries to readjust itself to the existing, almost frozen displacements of defects and very few defects change their sign.

The defects hinder the propagation of the deperiodization line of the stripple. Figure 17 illustrates such a process. At the edge on the right upper part of map 17(a), a half-stripple is seen. The stripple, map (b), tries to enter the crystallite but a group of defects does not let it through. This strained state lasts for some time, maps (c)—(d) and then a new stripple inside the system appears close to the previous one, map (e). The new stripple grows, maps (f)—(h), through the whole crystallite. The modulation wave vector k_p of the system, as detected by the diffuse scattering function, stays constant for some range of the k_p variation, because the propagation of the deperiodization line is hindered by the energy barriers introduced by the defects. That effect is responsible for the quasisteps observed, Fig. 15.

C. Order-disorder model

In the order-disorder model ($A_0 = -2.0$) the local field is a double minimum potential, therefore a process which needs particle transfer from one local minimum to another one may require some energy to overcome the barrier. That leads, for example, to an equilibrium relaxation time for this model which is slower than for the displacive one. Figure 18 shows the diffuse scattering distribution as a function of k_p. Contrary to the displacive case the satellites are often split. The positions of the maxima of the satellites for increasing and decreasing runs or the nonequilibrium devil's staircase curves are given in Fig. 19. Steplike behavior is observed and the steps are not related with any rational numbers except the strong one at $k_p = \frac{1}{4}$. The mechanisms of the wave vector k_p variation are similar to those of the displacive model. It was verified that within every quasistep the process is reversible. This follows from the fact that the propagation of the deperiodization line reverses when the increasing process of k_p is altered to a decreasing one, provided the deperiodization line has not yet disappeared.

The existence of the stripple in the finite crystallite may be interpreted as the coexistence of two modulations, of slightly different length. Thus, the diffuse scattering function may show the splitting of the satellite.

The increasing and decreasing runs presented in Figs. 11, 15, and 19 are not unique even when they are performed in very similar conditions. Figure 20 gives two decreasing runs for the order-disorder model with 2% of point defects. They are done with the same concentration and distribution of defects, the same rate dk_p/dt, the same temperature variation, but different starting equilibrated configurations at $k_p = 0.40$. In these two runs the sequence of quasisteps becomes different. The number of particles in real crystal is, of course, much larger than in our computer system. Therefore, the situation in real crystals is as follows. Regions of a crystal far apart from each other can be considered as independent subsystems, each having a particular sequence of quasisteps. Adding satellite intensities from all such regions, one averages them over different sequences of quasisteps and one could even obtain a continuous behavior of the $k_m = g(k_p)$ curve, except for parts of strong lock-in phases. In the experiment one observes the averaged satellite. The average curves will still show the global hysteresis. However, the

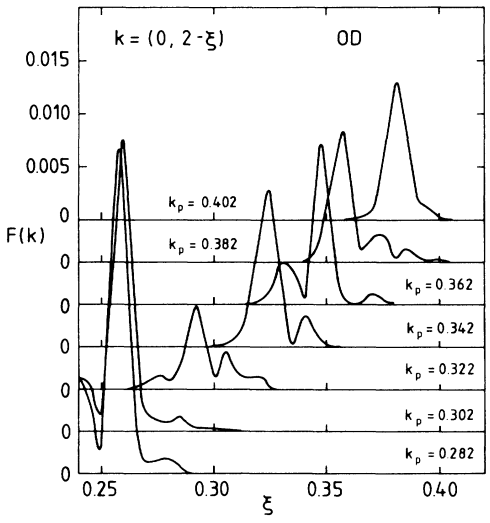

FIG. 18. Satellite behavior of the order-disorder model during the kinetic run as a function of the wave vector k_p which changes from 0.28 to 0.40. Points in Fig. 19 indicate the positions of maxima of these satellites.

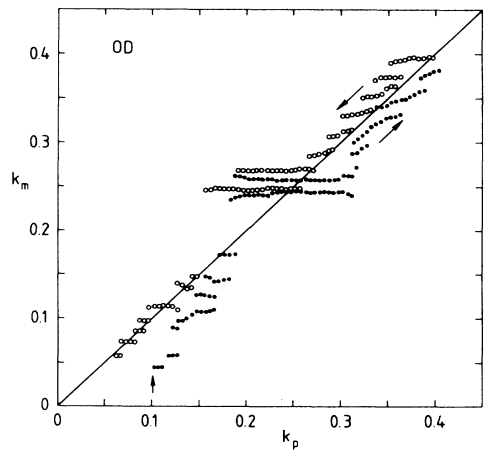

FIG. 19. Position of diffraction satellites in the order-disorder model detected by the diffuse scattering function $F(k)$ as a function of the wave vector k_p for a constant rate $dk_p/dt = \pm 4 \times 10^{-5}(1/\tau_0)$. Closed and open points correspond to $0.0 \rightarrow 0.4$ and $0.4 \rightarrow 0.0$ runs, respectively.

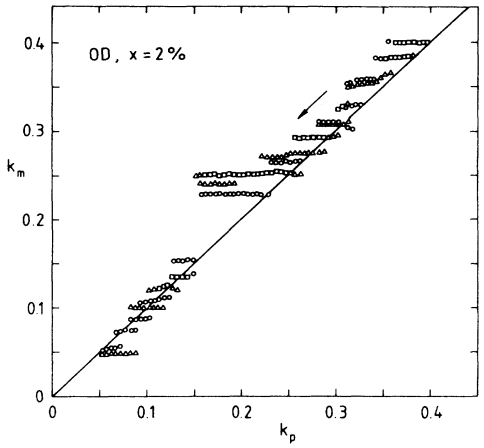

FIG. 20. The position of diffraction satellites for two similar runs in the order-disorder model with 2% of point defects detected by the diffuse scattering function $F(k)$ as a function of the wave vector k_p. The two runs are characterized by the same constant rate $dk_p/dt = -4\times10^{-5}(1/\tau_0)$ from 0.4 to 0.0, the same temperature variation but different starting equilibrated configurations. Circles and triangles correspond to the two runs, squares are common points of both runs.

steps can be observed by reversing the variation of k_p, or in real experiment by reversing the change of temperature and they recently have been observed by neutron diffraction experiment made on irradiated thiourea[10]

VIII. CONCLUSIONS

Our results confirm that the molecular-dynamics method enables one to simulate a large number of the properties of incommensurate phases. Our two-dimensional crystallite of 9409 particles with a polynomial potential energy and free boundary conditions showed a one-dimensional incommensurate modulation. Many processes, like the phase mode or nucleation and growth of stripple, need a second dimension in the system, which we have added. At $T=0$ our models were characterized by complete devil's staircases. Cooling runs proved the existence of the normal-to-incommensurate phase transitions. The cooling runs to $T=0$ indicated that the commensurate phase with domain walls can be achieved for potential energies characterized by a wave vector close to 0 or $\frac{1}{4}$. In other cases, instead of a commensurate phase, a nonperfect, although frozen, incommensurate phase was obtained. This was a consequence of a small driving force toward perfect incommensurate modulation in comparison with the temperature and the evolution time available in the simulation. In the diffraction pattern of the imperfect incommensurate modulation the intensities of the satellites, especially those of higher order, are considerably lower. Higher-order satellites may even disappear.

Our displacive model had a soft underdamped phonon mode. Let us recall that the model potential was temperature independent and the softening of the phonons occurred as a result of their renormalization by thermal fluctuations only. In the incommensurate phase we were able to distinguish between the phase and amplitude modes, and the phase-mode dispersion curve was gapless. Even after doping the crystallite with 2% substitutional point defects we did not see any influence on the phase-mode and amplitude-mode dispersion curves. The defects differed from the host particles in a local potential but not in the interparticle interaction.

Computer simulation makes it possible to study the behavior of the system as a function of the wave vector which specifies the minimum of the potential energy. By changing the potential parameters in time one can vary the characteristic wave vector of the modulation and study the nonequilibrium devil's staircase. Provided the system relaxes quickly to equilibrium, the nonequilibrium devil's-staircase curve at finite temperature is a continuous function except for wide lock-in phases. That is the case, at least partly, for the displacive model. When the characteristic relaxation time in the system, as in the order-disorder model, is considerably longer than the time available in the simulation, then the nonequilibrium devil's staircase consists of quasisteps which may not be related to any rational numbers. The processes along quasisteps are reversible. These quasisteps originate from the nucleation and growth of stripple. Runs with decreasing and increasing wave vectors clearly indicate the existence of global hysteresis.

The time scale in the numerical simulation is necessarily much shorter than in real experiments. However, the simultaneous study of displacive and order-disorder models shows that the characteristic relaxation times of the system, which is longer in the order-disorder case, plays a crucial role in the observed phenomena. One might expect similar effects in real samples, especially of the strongly order-disorder type, if one takes into account that the real experiment has a few orders of magnitude better resolution, that the sample is much larger than in the computer simulation and that real crystals contain defects which may increase some relaxation times considerably by pinning the deperiodization lines. Dielectric and neutron diffraction experiments made recently on irradiated thiourea samples[10] indicate that some phenomena reported here might be experimentally observed.

ACKNOWLEDGMENTS

The author wishes to thank H. Grimm for numerous and valuable discussions. Fruitful comments by T. Springer, H. Stiller, M. Lambert, F. Denoyer, R. A. Cowley, G. S. Pawley, J. Villain, and K. Wingerath are gratefully acknowledged. The author would like to express thanks to the staff of Institut für Festkörperforschung, Kernforschungsanlage, Jülich, for their hospitality and assistance.

*Permanent address: Institute of Nuclear Physics, ulica Radzikowskiego 152, PL-31-342 Kraków, Poland.

[1]S. Aubry and P. Y. Le Daeron, Physica D **8**, 381 (1983).

[2]T. Janssen, in *Incommensurate Phases in Dielectrics,* Vol. 14 of *Modern Problems in Condensed Matter Sciences,* edited by R. Blinc and A. P. Levanyuk (North-Holland, Amsterdam, 1986), Part 1, Chap. 3.

[3]K. Parlinski and K. H. Michel, Phys. Rev. B **29**, 396 (1984).

[4]M. Iizumi and K. Gesi, J. Phys. Soc. Jpn. **16**, 3254 (1983).

[5]F. Dénoyer and R. Currat, in *Incommensurate Phases in Dielectrics,* Vol. 14 of *Modern Problems in Condensed Matter Sciences,* Ref. 2, Part 2, Chap. 4.

[6]G. Marion, R. Almairac, M. Ribet, U. Steigenberger, and C. Vettier, J. Phys. **45**, 929 (1984).

[7]E. Fjaer, R. A. Cowley, and T. W. Ryan, J. Phys. C **18**, L-41 (1985).

[8]G. Dolino, in *Incommensurate Phases in Dielectrics,* Vol. 14 of *Modern Problems in Condensed Matter Sciences,* Ref. 2, Part 2, Chap. 16.

[9]H. G. Unruh, J. Phys. C **16**, 3254 (1983).

[10]G. André, D. Durand, F. Dénoyer, R. Currat, and F. Moussa, Phys. Rev. B **35**, 2909 (1987).

[11]J. P. Jamet and P. Lederer, J. Phys. (Paris) **44**, L-257 (1983).

[12]H. Cailleau, in *Incommensurate Phases in Dielectrics,* Vol. 14 of *Modern Problems in Condensed Matter Sciences,* Ref. 2, Part 2, Chap. 12.

[13]R. Blinc, Phys. Rep. **79**, 332 (1981).

[14]K. Parlinski, J. Phys. C **18**, 5667 (1985).

[15]K. Parlinski and F. Denoyer, J. Phys. C **18**, 293 (1985).

[16]S. Aubry in *Soliton in Condensed Matter,* Vol. 8 of *Solid State Sciences,* edited by A. R. Bishop and T. Schneider (Springer, Berlin, 1978) p. 264.

[17]K. Parlinski and H. Grimm, Phys. Rev. B **33**, 4868 (1986).

[18]L. Bernard, R. Currat, P. Delamoye, C. M. E. Zeyen, S. Hubert, and R. de Kouchkovsky, J. Phys. C **16**, 433 (1983).

[19]V. Janovec, Phys. Lett. **99A**, 384 (1983).

[20]K. Kawasaki, J. Phys. C **16**, 6911 (1983).

[21]K. K. Fung, S. McKernan, J. W. Steeds, and J. A. Wilson, J. Phys. C **14**, 5417 (1981).

[22]P. Prelovšek and T. M. Rice, J. Phys. C **16**, 6513 (1983).

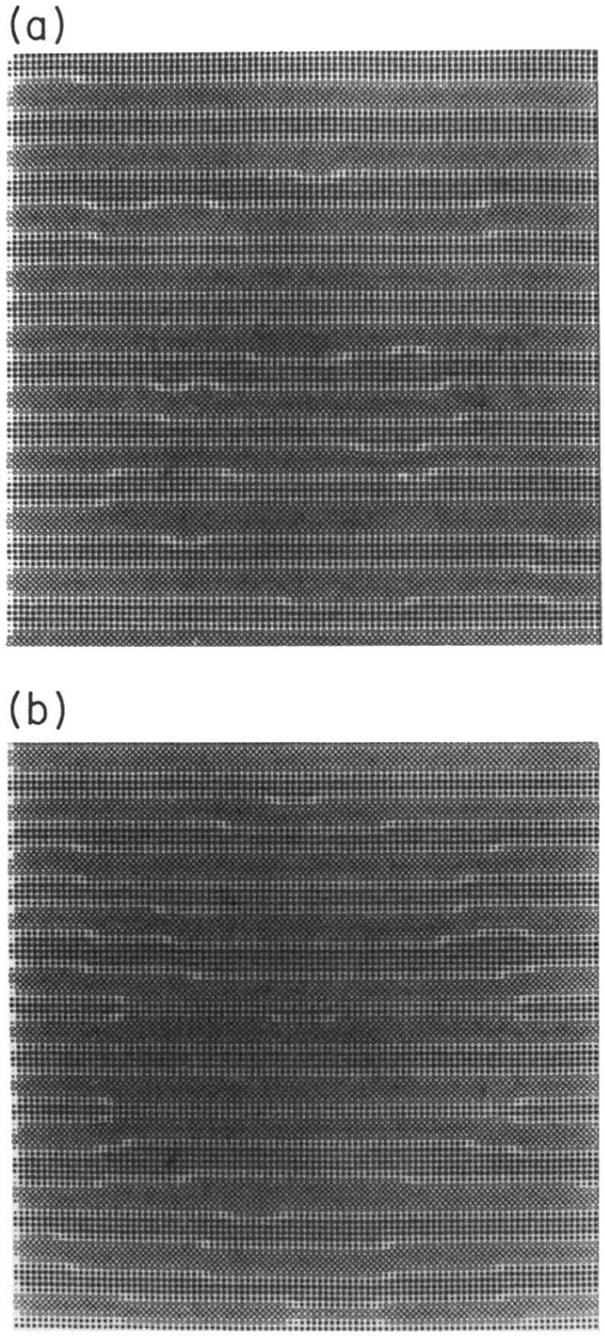

FIG. 4. Configuration of particles of an order-disorder model at $T=0$ for (a) $k_p=0.10$ and (b) $k_p=0.11$.